Submitted to: Journal of
Computer Methods in Applied
Mechanics and Engineering

Modeling of Oxidation and its Effect on Crack Growth in Titanium Alloys

Dimitris C. Lagoudas, Pavlin Entchev and
Robertus Triharjanto

*Center for Mechanics of Composites, Department of Aerospace Engineering ,
Texas A&M University, College Station, TX 77843-3141*

Abstract

The effect of oxidation on the crack growth resistance of titanium alloys is investigated in this work. The oxidation process is modeled by modifying the Fickian diffusion problem in order to account for the chemical reaction (phase change) in the material. Two different variants of a fixed grid finite element method for numerical simulation of oxidation are used. The first approach taken is to locate the oxidation front and split the domain into metal and oxide subdomains. The second approach is based on reformulating the diffusion equations in both the oxide and metal, resulting in a single non-linear equation for the whole domain. After the oxidation process is modeled, the mechanical analysis is performed. In the finite element formulation of the mechanical problem, the influence of oxidation is introduced by the change of the elastic constants and the oxidation-induced eigenstrain. The applicability of both the oxidation and mechanical models is tested by simulating oxidation of a pre-cracked Ti-15-3 compact tension specimen which is then subjected to monotonic loading.

1 Introduction

Titanium alloys and titanium-based Metal Matrix Composites (MMC) have been proposed for elevated temperature applications because of their high strength and ability to retain mechanical integrity in harsh environments. Applications anticipated for structural components in advanced turbine engines and hypersonic aircraft require the structural member to withstand severe mechanical loading and temperature variations. Experimental studies have shown that the mechanical loading and oxidation significantly damage titanium alloys [1,2,3,4,5,6,7]. These studies show that oxidation degrades the composite due to the

development of a brittle TiO_2 layer. One common reason cited for the degradation of properties of SiC/Ti MMCs at elevated temperature is attributable to the SiC fibers which serve to facilitate the flow of oxygen along the fiber-matrix interface which in turn embrittles the matrix material [8,9,10]. However, researchers [11,12,13,14], to name just a few, believe that the high oxygen diffusivity rate of titanium alloys is really the core issue to be addressed. The aforementioned researchers have carefully shown the influence that environment has on the mechanical behavior of the material systems investigated. The experimental work [14] examines the influence of temperature, stress range and environment on the fatigue performance of SCS-6/Ti-22Al-23Nb composite. Fatigue life of specimens tested in high vacuum have been compared to those tested at the same temperature and stress level in air. The results of this study indicate an order of magnitude increase in life for specimens tested in vacuum, indicating a strong influence of an oxidizing environment on fatigue life. Fatigue crack growth in Ti-46.4Al-3Nb-2Cr-0.2W specimens [13] over a wide temperature range in laboratory air and ultra high vacuum (UHV) show that crack growth rates are over an order of magnitude slower in UHV as compared to laboratory air. This effect has been explained to be caused by an oxygen embrittlement of the alloy.

However, another experimental study [15] has shown that oxidation during fatigue crack growth experiments of $\mathrm{Ti} - \beta 21\mathrm{S}$ improves the material performance by reducing the fatigue crack growth rate.

The objective of this research effort is to model the oxidation process of titanium alloys and evaluate its effect on the crack growth resistance of the metal. In addition, it will provide a valuable insight as to how oxidation actually effects the mechanical performance of damaged titanium alloys. The modeling effort is separated into two parts, i.e., modeling the oxidation of titanium alloys and modeling its effect on crack growth resistance.

Figure 1 shows SEM photographs of an oxidized titanium wire and an oxidized crack tip in titanium. These experiments were performed at the Materials and Structures Laboratory at Texas A&M University. These and other similar experimental observations have motivated the authors to focus on the modeling of oxidation in 2D domains, beyond the traditional 1D analysis. Modeling of the oxidation near the crack tip is of particular interest, since this kind of problem arises in critical engineering applications associated with damage in titanium matrix composites.

Modeling the oxidation of titanium alloys and tracking the oxidation front involves the development of numerical techniques similar to the ones used for phase change problems. Such techniques can generally be divided into two groups. The first group consists of algorithms with explicit capturing of the unknown phase change interface [16,17,18,19,20]. The second group includes methods without explicit interface tracking which are based on smearing the free boundary [21]. This research investigates applications of the methods belonging to both groups. The first approach tracks the oxidation front and splits the domain into metal and oxide subdomains. The second approach is based on reformulating the governing partial differential equations (PDEs) in both the oxide and metal regions, resulting in a single nonlinear PDE for the whole domain. Both methods are numerically implemented using the

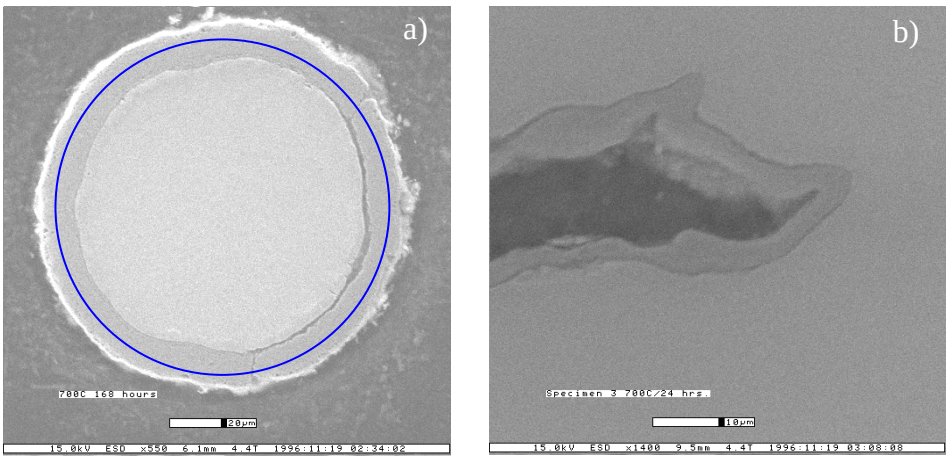

Fig. 1. a) Titanium wire oxidized at 700°C for 168hr; b) Crack tip in titanium oxidized at 700°C for 24hr.

finite element method (FEM).

Two of physical characteristics of the oxide scale (i.e., the stiffness change and the volumetric expansion) have an impact on the mechanical response of the metal. The stiffness change is a result of the metal being transformed into oxide compound; whereas, the volumetric expansion is due to the porosity of TiO_2 and its lower density compared to titanium. The volumetric expansion of the oxide scale is shown in Fig.1a for titanium wire, where the dark circle indicates the initial diameter of the wire.

The method used in this work for calculating the energy release rate is the crack closure method. This method [22] is based on the premise that the energy required to propagate the crack is equal to the energy required to close the crack to its original length; and, it is applicable to both homogeneous and heterogeneous materials.

Both the oxidation and the mechanical models are validated by comparing the results with analytical solutions for selected test cases. After validating the numerical methods, the oxidation and mechanical models are combined to evaluate the effect of oxidation on the energy release rate of a Ti-15-3 compact tension specimen.

The remainder of the paper is organized as follows: the next section presents a 2D Fickian diffusion model of oxidation with a moving interface. Section 3 is devoted to the numerical solution for the oxidation problem. Section 4 discusses energy release rate of Ti-15-3 compact tension specimens and Section 5 is devoted to conclusions.

2 Two-Dimensional Fickian Diffusion Model of Oxidation with a Moving Interface

Let $\Omega \subset \mathbb{R}^2$ be a fixed domain with $\partial\Omega$ as its boundary. Ω is partitioned by the interface curve $\tau(t)$ with parameterization $\mathbf{r}(s,t)$, $s_1(t) \leq s \leq s_2(t)$ into two subdomains Ω_1 and Ω_2, respectively, such that $\Omega = \Omega_1 \cup \Omega_2$, $\tau = \Omega_1 \cap \Omega_2$, and $\partial\Omega = \partial\Omega_1 \cup \partial\Omega_2$ (Fig.2).

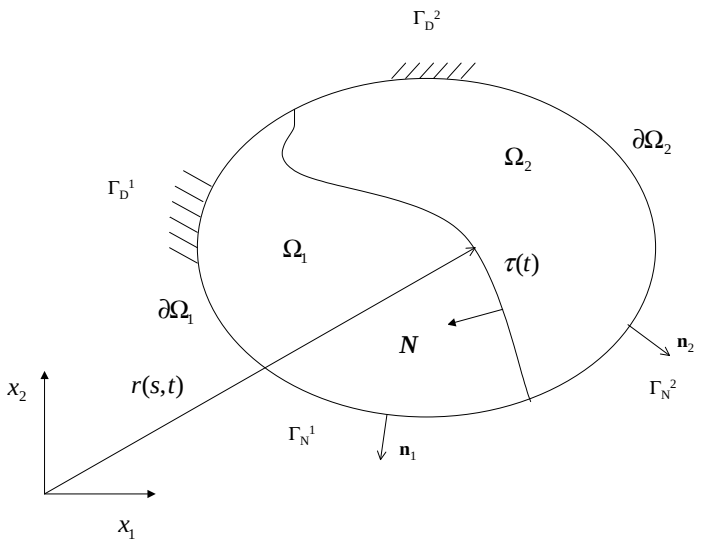

Fig. 2. Two-Dimensional domain with interface $\tau(t)$ separating two different phases which occupy Ω_1 and Ω_2, respectively.

Assuming that Fickian diffusion is valid, the total mass concentration of oxygen in Ω_1 and Ω_2 satisfies the following equations [23] :

$$\frac{\partial c_1(\mathbf{x},t)}{\partial t} = \nabla \cdot (D_1 \nabla c_1(\mathbf{x},t)), \quad \mathbf{x} \in \Omega_1, \tag{1}$$

$$\frac{\partial c_2(\mathbf{x},t)}{\partial t} = \nabla \cdot (D_2 \nabla c_2(\mathbf{x},t)), \quad \mathbf{x} \in \Omega_2. \tag{2}$$

Here $c_1(\mathbf{x},t)$ and $c_2(\mathbf{x},t)$ are the total mass concentrations of oxygen in Ω_1 and Ω_2, respectively, and D_1 and D_2 are the diffusivities of the two phases (i.e., oxide scale and titanium matrix) that occupy Ω_1 and Ω_2 , respectively.

The initial conditions are

$$c_1(\mathbf{x},0) = f_1 \quad \mathbf{x} \in \Omega_1(t), \tag{3}$$

$$c_2(\mathbf{x},0) = f_2 \quad \mathbf{x} \in \Omega_2(t) \text{ and} \tag{4}$$

$$\mathbf{r}(s,0) = \mathbf{r}_0(s). \tag{5}$$

The boundary conditions on $\partial\Omega$ are

$$c_1(\mathbf{x},t) = \hat{c}_1(\mathbf{x},t) \quad \text{on} \quad \Gamma_D^1 \quad \text{and} \quad -D_1\nabla c_1 \cdot \mathbf{n}_1 = \hat{m}_1^n(\mathbf{x},t) \quad \text{on} \quad \Gamma_N^1, \tag{6}$$

$$c_2(\mathbf{x},t) = \hat{c}_2(\mathbf{x},t) \quad \text{on} \quad \Gamma_D^2 \quad \text{and} \quad -D_2\nabla c_2 \cdot \mathbf{n}_2 = \hat{m}_2^n(\mathbf{x},t) \quad \text{on} \quad \Gamma_N^2, \tag{7}$$

where $\hat{c}_1(\mathbf{x},t)$, $\hat{c}_2(\mathbf{x},t)$ are prescribed oxygen concentrations. $\hat{m}_1^n(\mathbf{x},t)$, and $\hat{m}_2^n(\mathbf{x},t)$ are normal components of oxygen mass flux through the external boundaries of Ω_1 and Ω_2 for $t > 0$, with outward unit normal vectors $\mathbf{n}_1$ and $\mathbf{n}_2$ and

$$\partial\Omega_1 = \Gamma_D^1 \cup \Gamma_N^1, \quad \partial\Omega_2 = \Gamma_D^2 \cup \Gamma_N^2. \tag{8}$$

The interface $\tau(t)$ that partitions Ω into two regions is a phase boundary that separates the oxidized part from the metallic part, where oxidation has not taken place. Assuming that the chemical reaction occurs on a short time scale compared with the diffusion process, when the concentration of oxygen reaches a critical value c_{cr}, oxidation instantaneously takes place and the interface moves, always satisfying the critical concentration requirement. The appropriate interface conditions, expressing conservation of total oxygen mass across the interface and initiation of the oxidation process whenever a critical oxygen concentration is reached, are given by

$$-D_1(\nabla c_1)\cdot\mathbf{N} = -D_2(\nabla c_2)\cdot\mathbf{N} + [c]\,V, \tag{9}$$

$$c_1(r,t) = c_{cr} \quad , \quad c_2(r,t) = c_{cr} - [c], \tag{10}$$

where $\mathbf{N}$ is the unit normal vector on $\tau(t)$ pointed outward Ω_2, V is the normal velocity of the oxidation interface, namely, $V = \frac{d\mathbf{r}}{dt}\cdot\mathbf{N}$ and $[c]$ is the jump discontinuity of the oxygen concentration at the interface.

3 Numerical Simulation of Oxidation Process

3.1 Discrete Interface Method

The discrete interface method belongs to the group of front tracking methods, whereby the location of the moving interface is found by solving the oxygen diffusion equations in domains adjacent to the interface and by connecting the solution through appropriate interface conditions. The discrete interface formulation starts by multiplying the governing equations (1),(2) in two phases with the test function φ and integrating over the region Ω, i.e.,

$$\int_{\Omega_1} D_1\nabla^2 c_1\varphi dA + \int_{\Omega_2} D_2\nabla^2 c_2\varphi dA = \int_{\Omega} \varphi\left(\frac{\partial c_1}{\partial t} + \frac{\partial c_2}{\partial t}\right) dA. \tag{11}$$

Performing integration by parts and considering the interface condition (9), the above equation yields

$$\sum_{\alpha=1}^{2} \int_{\Omega_\alpha} \left(D_\alpha \nabla\varphi \cdot \nabla c_\alpha - \varphi \frac{\partial c_\alpha}{\partial t} \right) dA = \sum_{\alpha=1}^{2} \int_{\partial\Omega_\alpha - \tau} \varphi D_\alpha \nabla c_\alpha \cdot \mathbf{N} ds + \int_{\tau} \varphi [c] V ds. \tag{12}$$

Applying the Galerkin method (i.e., use a similar shape function for the concentration and the test function), equation (12) can be rewritten as

$$\sum_{\alpha=1}^{2} \int_{\Omega_\alpha} \left(D_\alpha \nabla\varphi \cdot \nabla c_\alpha - \varphi \frac{\partial c_\alpha}{\partial t} \right) dA = \int_{\tau} \varphi [c] V ds, \tag{13}$$

and

$$c(\mathbf{x}) = \sum_{i=1}^{N} c_i \varphi_i,$$

where $\{\varphi\}$ are the shape functions and c_i are the nodal concentration values. Using linear interpolation in time (which is a standard procedure for the time dependent finite element problem [24]), the concentration at any time point can be expressed as

$$\{c_\alpha\} = (1-\theta)\{c_\alpha^n\} + \theta\{c_\alpha^{n+1}\}, \quad 0 \le \theta \le 1, \quad \alpha = 1, 2. \tag{14}$$

Using (14) and a finite difference approximation for the time derivative, the equation (13) can be rewritten as

$$\sum_{\alpha=1}^{2} \left[-\frac{\mathbf{M}_\alpha^{n+1}}{\Delta t} + \theta \mathbf{K}_\alpha^{n+1} \right] \mathbf{c}_\alpha^{n+1} = \sum_{\alpha=1}^{2} \left[-\frac{\mathbf{M}_\alpha^{n}}{\Delta t} + \theta \mathbf{K}_\alpha^{n} \right] \mathbf{c}_\alpha^{n} + \mathbf{F}^n, \tag{15}$$

where

$$K_{\alpha_{ij}} = \int_{\Omega_\alpha} D_\alpha \nabla\varphi_i \cdot \nabla\varphi_j dA, \tag{16}$$

$$M_{\alpha_{ij}} = \int_{\Omega_\alpha} \varphi_i \cdot \varphi_j dA, \tag{17}$$

$$F_i = \int_{\tau} [c] \varphi_i V ds = \frac{1}{\Delta t} \int_{\Omega_m} [c] \varphi_i dA, \tag{18}$$

and Ω_m is the area swept by the interface during its propagation in time Δt.

An iterative approach is necessary in order to solve equation (15) since it has 2 interdependent variables. The solution strategy starts with guessing the interface location for the next time increment so that $\mathbf{M}_\alpha^{n+1}$ and $\mathbf{K}_\alpha^{n+1}$ can be evaluated. After solving the linear system,

the interface location is calculated by interpolating the nodal concentration $\mathbf{c}_\alpha^{n+1}$. The iterative process is ended when the difference between the interface location used to calculate $\mathbf{M}_\alpha^{n+1}$ and $\mathbf{K}_\alpha^{n+1}$ and the interface location obtained by interpolating $\mathbf{c}_\alpha^{n+1}$ is smaller than a prescribed error limit.

3.2 Interface Smearing Method

To avoid dealing with the jump discontinuity, the following change of variables is introduced:

$$\overline{c_2}\left(\mathbf{x},t\right)=c_2\left(\mathbf{x},t\right)+\left[c\right]. \tag{19}$$

The single diffusivity coefficient D is introduced by the following equality:

$$D\left(c\right)=\begin{cases} D_1, & \text{if} \quad c>c_{cr}, \\ D_2, & \text{if} \quad c<c_{cr}. \end{cases} \tag{20}$$

By including condition (9) in the governing equations (1) and (2), we obtain

$$\left\{1+\left[c\right]\delta\left(c-c_{cr}\right)\right\}\frac{\partial c}{\partial t}=\nabla\cdot\left(D\left(c\right)\nabla c\right), \tag{21}$$

where

$$c=\begin{cases} c_1, & \text{if} \quad c>c_{cr}, \\ \overline{c_2}, & \text{if} \quad c<c_{cr}. \end{cases}$$

Equation (21) combines the governing equations (1) and (2), as well as the interface condition (9). The equivalence of the above two systems of equations is considered in detail in [21]. To avoid dealing with the Dirac function, the smoothed function $\tilde{\delta}\left(c-c_{cr},\Delta\right)$ is introduced (Δ is the extent of a semi-interval for concentration c in which $\tilde{\delta}\left(c-c_{cr},\Delta\right)\neq 0$). The coefficient $\tilde{G}\left(c\right)$ is introduced by the following equality:

$$\tilde{G}\left(c\right)=1+\left[c\right]\tilde{\delta}\left(c-c_{cr},\Delta\right). \tag{22}$$

In the interval $\left(c_{cr}-\Delta,c_{cr}+\Delta\right)$, the coefficient $D\left(c\right)$ is approximated by a linear function, i.e.,

$$\tilde{D}\left(c\right)=\begin{cases} D_1, & \text{if} \quad c>c_{22}, \\ \dfrac{D_1-D_2}{2\Delta}c+\dfrac{D_2c_{22}-D_1c_{11}}{2\Delta}, & \text{if} \quad c_{11}\leq c\leq c_{22}, \\ D_2, & \text{if} \quad c<c_{11}, \end{cases} \tag{23}$$

where

$$c_{11} = c_{cr} - \Delta, \quad c_{22} = c_{cr} + \Delta.$$

By combining equations (21), (22) and (23), the following equation is obtained:

$$\tilde{G}(c)\frac{\partial c}{\partial t} = \nabla \cdot \left(\tilde{D}(c)\nabla c\right). \tag{24}$$

As a result of the above problem reformulation, we have to solve a single non-linear PDE (24) instead of solving equations (1), (2) and (9).

Multiplying (24) by the test function φ and integrating over the domain Ω for a fixed time t, we have:

$$\int_{\Omega} \tilde{G}(c)\frac{\partial c}{\partial t}\varphi dA = \int_{\Omega} \nabla \cdot \left(\tilde{D}(c)\nabla c\right)\varphi dA. \tag{25}$$

By applying Green's formula, the right-hand side term in the above equation becomes

$$\int_{\Omega} \tilde{G}(c)\frac{\partial c}{\partial t}\cdot\varphi dA + \int_{\Omega} \tilde{D}\nabla c\cdot\nabla\varphi dA - \int_{\partial\Omega} \tilde{D}\frac{\partial c}{\partial n}\varphi ds = 0. \tag{26}$$

Assuming

$$\frac{\partial c}{\partial n} = 0 \quad \text{on} \quad \Gamma_N$$

and following the standard Galerkin procedure, the weak formulation of the problem for fixed t becomes

$$\int_{\Omega} \tilde{G}(c)\frac{\partial c}{\partial t}\cdot\varphi dA + \int_{\Omega} \tilde{D}\nabla c\cdot\nabla\varphi dA = 0, \quad t > 0, \tag{27}$$

where φ is in the space of piecewise linear functions. Using the standard FEM approach, the oxygen concentration is given by

$$c(\mathbf{x}, t) = \sum_{i=1}^{N} c_i(t)\varphi_i(\mathbf{x}), \tag{28}$$

where $c_i(t)$ are the nodal values of oxygen concentration. Substituting (28) into (27) and enforcing equation (27) for all test functions φ_j, we have:

$$\mathbf{M}\frac{d\mathbf{c}}{dt} + \mathbf{K}\mathbf{c} = 0, \tag{29}$$

where $\mathbf{K}$ and $\mathbf{M}$ are corresponding "stiffness" and "mass" matrices with entries

$$M_{ij} = \int_{\Omega} \tilde{G}\varphi_j\varphi_i dA, \tag{30}$$

$$K_{ij} = \int_{\Omega} \tilde{D}\nabla\varphi_j \cdot \nabla\varphi_i dA. \tag{31}$$

Using the backward Euler method for the time derivative in the semi-discrete problem given by (29), we obtain

$$\mathbf{M}\frac{\mathbf{c}^n - \mathbf{c}^{n-1}}{\Delta t} + \mathbf{K}\mathbf{c}^n = 0, \tag{32}$$

where $\mathbf{c}^n$ and $\mathbf{c}^{n-1}$ are the evaluations of $\mathbf{c}$ at the n^{th} and $(n-1)^{th}$ time steps and Δt is the time increment. For a given $\mathbf{c}^{n-1}$, equation (32) results in the following system of equations for the unknown $\mathbf{c}^n$:

$$\left(\frac{\mathbf{M}}{\Delta t} + \mathbf{K}\right)\mathbf{c}^n = \frac{\mathbf{M}}{\Delta t}\mathbf{c}^{n-1}. \tag{33}$$

Note that matrices $\mathbf{M}$ and $\mathbf{K}$ include the non-linear coefficients $\tilde{G}(\mathbf{c})$ and $\tilde{D}(\mathbf{c})$. Therefore, an iterative process is used to solve (33). The iterative process uses the value of $\mathbf{c}$ from the previous iteration and terminates when the maximum difference between two successive iterative solutions is less than a desired tolerance in the domain.

3.3 Numerical results

To validate the aforementioned numerical algorithms for 2D problems, the following test case is presented. We consider a square domain $\Omega = \{(x_1, x_2) : 0 \leq x_1 \leq 100\mu m, 0 \leq x_2 \leq 100\mu m\}$ with the following boundary and initial conditions:

$$c(\mathbf{x}, t) = c_0, \quad \mathbf{x} \in \Gamma_D \quad \text{and} \quad \frac{\partial c}{\partial n} = 0, \quad \mathbf{x} \in \Gamma_N, \tag{34}$$

$$c(\mathbf{x}, 0) = 0, \tag{35}$$

where $\Gamma_D = \{(x_1, x_2) : x_1 = 0, 0 \leq x_2 \leq 100\mu m\}$ and $\Gamma_N = \partial\Omega \setminus \Gamma_D$.

The above formulated 2D problem is equivalent to the 1D problem in x_1 direction, since the resulting concentration is independent on x_2. The analytical solution for the 1D problem given in [25] is used in this work for comparison purposes. The oxide layer thickness vs.

time computed by the two different finite element methods discussed earlier, as well as the analytical solution, are plotted in Fig.3a. In addition, an SEM photograph showing the oxide scale formed on Ti-15-3 specimen for 3 hours of oxidation is shown in Fig.3b. The following parameters, corresponding to Ti-15-3 oxidized at 700°C [23], have been used: $D_1 = 3.02{\cdot}10^{-3}\mu m^2/sec, D_2 = 1.431{\cdot}10^{-3}\mu m^2/sec, c_{cr} = 0.65{\cdot}c_0$ and $[c] = 0.5{\cdot}c_0$. As may

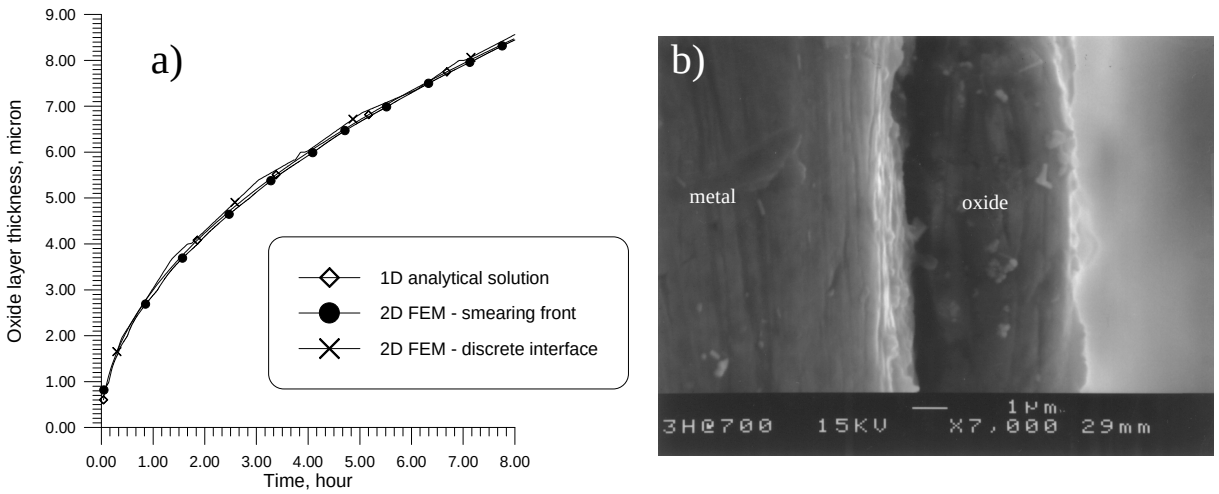

Fig. 3. Oxide layer growth in Ti-15-3: a) modeling results; b) SEM photograph of the oxide layer on Ti-15-3 formed at 700°C for $3hrs$ [23].

be seen from Fig.3, both approaches are in agreement with the analytical solution and with experimental data. The above level of accuracy has been observed for the time increment $\Delta t = 10sec$ and a mesh of triangular elements with element size $1\mu m$.

The numerical methods described in sections 3.1 and 3.2 have also been compared with the analytical solution of a problem of the oxide layer growth from the surface of a semi-infinite crack (see Fig.4). For comparison purposes it is be assumed that $D_1 = D_2 = D$ and $[c] = 0$, since for this case the problem has an analytical solution [26]. A finite square domain with dimensions $100\mu m{\times}100\mu m$ is used for computations and the oxidation time is such that the oxide growth is not affected by the presence of the finite external boundaries. The crack length a is assumed to be equal to $30\mu m$ for the numerical calculations. Results that compare the analytical solution and the two FEM solutions are shown in Fig.5 and Fig.6. Oxygen concentration profiles perpendicular to the crack surface along the x_2 axis (for $x_1 = 0$) are plotted in Fig.5 and profiles ahead of the crack tip (for $x_2 = 0$, $x_1 \geq a$) are plotted in Fig.6. As may be seen in both of these figures, the numerical results obtained with either approach are in agreement with the analytical solution.

Having gained experience in terms of discretization in space and time from the above example problem, we now consider a realistic case wherein the oxide layer will propagate from a crack surface in Ti-15-3 such that $D_1 \neq D_2$ and the concentration jump is non-zero. The material parameters corresponding to Ti-15-3 at 700°C [23] have been used for the numerical solution of this problem. For the purpose of this analysis, a square Ti-15-3 specimen $15\mu m{\times}15\mu m$ with a crack length $8\mu m$ has been considered. The location of the oxidation front at times $0.25hr$, $0.5hr$ and $1hr$ is plotted in Fig.7. Direct comparison with experimental results for

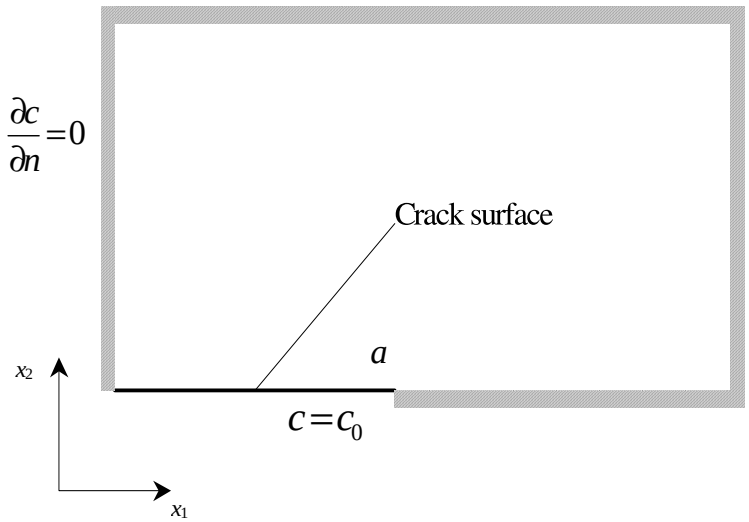

Fig. 4. Schematic of the geometry for the oxidation from a crack surface.

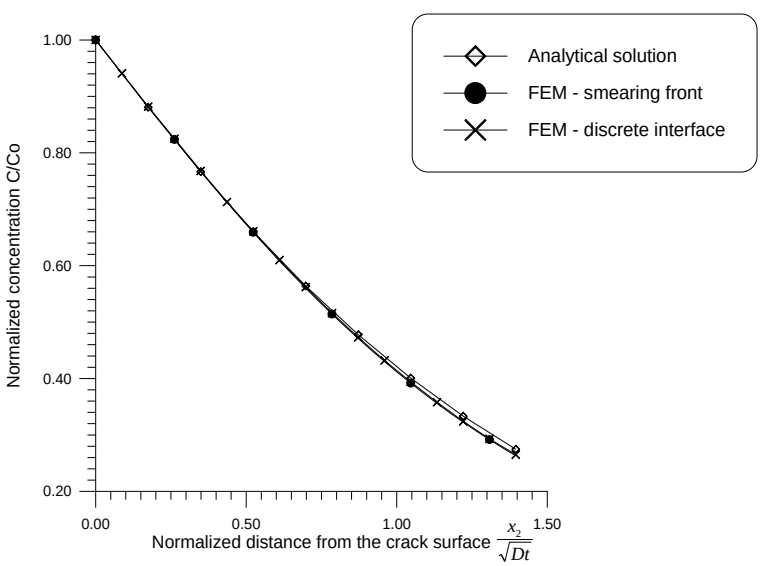

Fig. 5. Oxygen concentration profiles along x_2 perpendicular to the crack surface ($x_1 = 0$) for test case shown in Fig.4.

this case is very difficult, since the surface crack appears to be non-planar at a length scale comparable with oxide layer thickness, as seen in Fig.1b.

4 Energy Release Rate of Preoxidized Ti-15-3 Compact Tension Specimens

Having developed tools to numerically solve the oxidation problem, the effect of oxidation on the energy release rate of Ti-15-3 compact tension specimens under Mode I monotonic

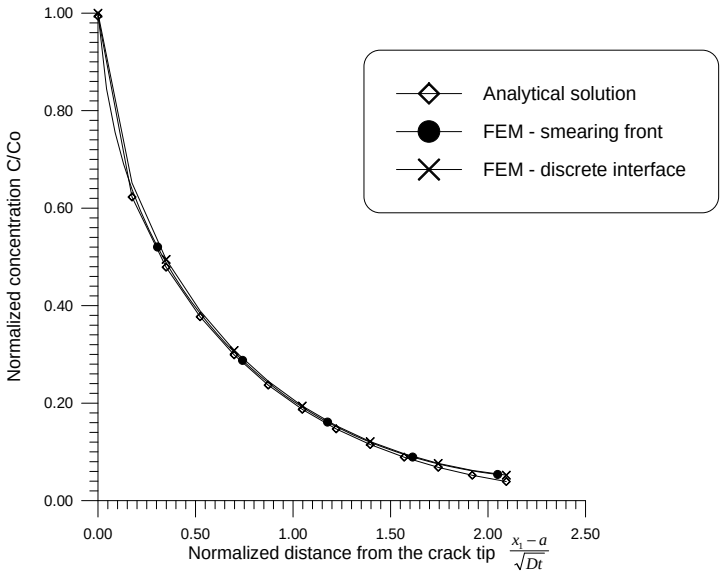

Fig. 6. Oxygen concentration profiles ahead of the crack tip

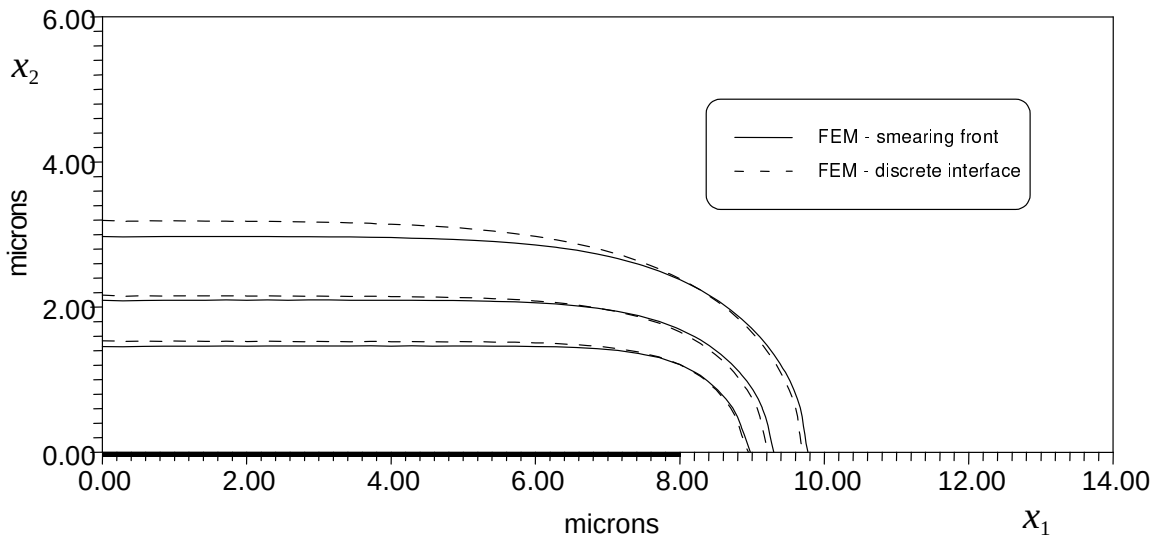

Fig. 7. Simulation of the location of oxidation front in an oxidized Ti-15-3 specimen at 700°C.

loading (see Fig.8a) will be modeled in this section. The assumptions that are made in order to solve this particular problem are:

(1) Given that the specimen was oxidized at an elevated temperature (700°C) and the mechanical loading is applied at lower temperature, it is assumed that the material behavior for both the oxide and the metal is elastic. In addition, isotropic linear behavior is assumed;
(2) Since the thickness of the oxide layer is considerably smaller than the typical thickness of the metallic specimen, plane strain condition is assumed.

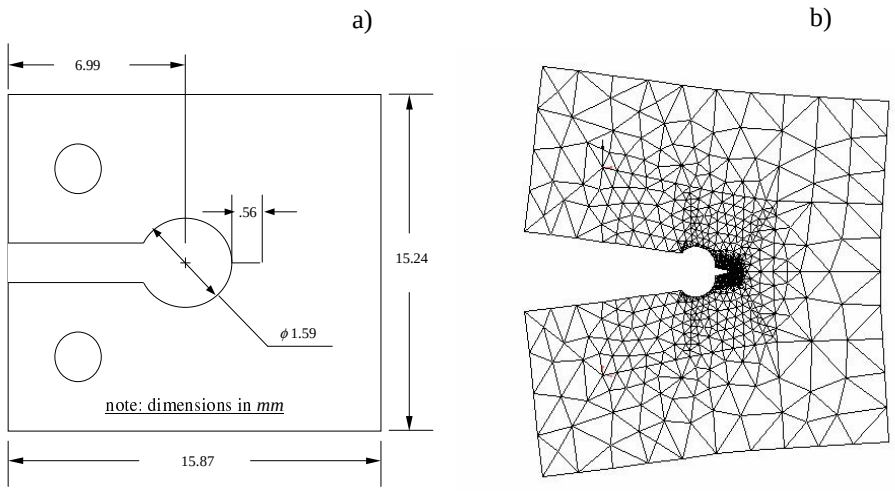

Fig. 8. Standard compact tension specimen.

Growth of the oxide layer has been modeled using the interface smearing method, described in Section 3. Results, shown in Fig.7 suggest the configuration of the oxide layer near the crack tip. Following these results, the structure of the finite element mesh near the crack tip has been chosen as shown in Fig.9.

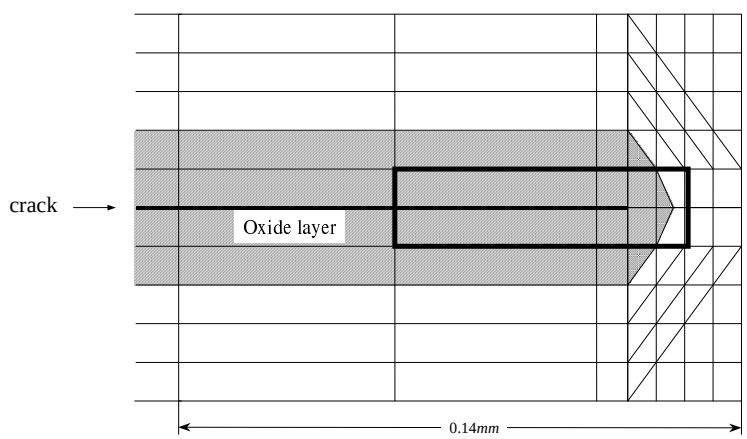

Fig. 9. Configuration of the FEM mesh near the crack tip.

Two methods have been widely used for finding the energy release rate in fracture mechanics problems; namely, the isoparametric method [27] and the crack closure method [22]. The isoparametric method computes the J-integral which is equal to the energy release rate [28]. The crack closure method is based on the contention that if a crack extends by a small length Δc, the energy absorbed in the process is equal to the work required to close the crack to its original length [22].

The reader should be aware of the fact that the J-integral is independent of the integration path only in case of a homogeneous material [29,30]. To briefly show this, consider the closed path $\Gamma^* = \Gamma_1 + \Gamma_2$+crack surfaces (see Fig.10) for a crack along x_1 axis. By evaluating

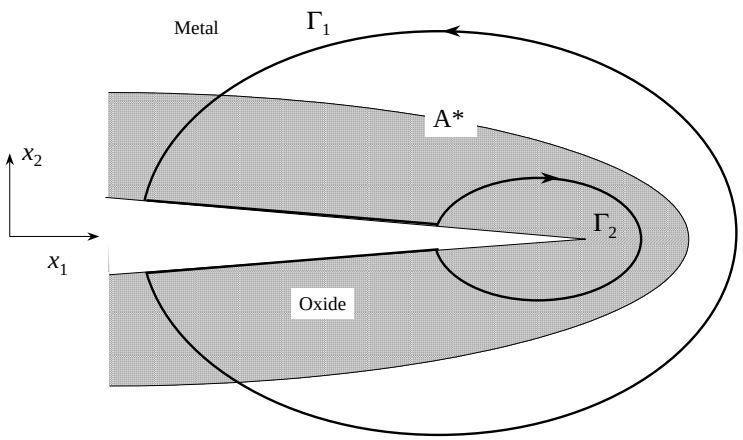

Fig. 10. Schematic representation of an oxidated cracked specimen with partial oxidation of the crack surfaces.

the J-integral on Γ^* and applying the divergence theorem, the expression for the J-integral becomes

$$J_{\Gamma^*} = \int_{\Gamma^*} \left(W dx_2 - t_i \frac{\partial u_i}{\partial x_1} ds \right) = \int_{A^*} \left[\frac{\partial W}{\partial x_1} - \frac{\partial}{\partial x_j} \left(\sigma_{ij} \frac{\partial u_i}{\partial x_1} \right) \right] dA, \tag{36}$$

where $W(x_i)$ is the strain energy density for a general inhomogeneous elastic material. Noting that

$$\frac{\partial W}{\partial x_1} = \frac{\partial \hat{W}}{\partial x_1} + \frac{\partial \hat{W}}{\partial \varepsilon_{ij}} \frac{\partial \varepsilon_{ij}}{\partial x_1}, \tag{37}$$

where $W(x_i) = \hat{W}(x_i, \varepsilon_{ij}(x_k))$, equation (36) yields

$$J_{\Gamma^*} = J_{\Gamma_1} - J_{\Gamma_2} = \int_{A^*} \frac{\partial \hat{W}}{\partial x_1} dA, \tag{38}$$

which leads to conclusion that the J-integral is independent of the path only if the material is homogeneous along the material direction x_1. Therefore, for the problem considered herein, that is one involving material inhomogeneities due to the presence of oxide scale at the surface of the crack, the isoparametric formulation will not be applicable. A note on special cases where the isoparametric method can be applied for heterogeneous materials is presented in

the Appendix. Hence, we will only consider the crack closure method which is not influenced be the presence of inhomogeneities.

For the crack closure method and Mode I loading, the energy release rate can be expressed using a polar coordinate system with the origin at the extended crack tip as [22]

$$\mathcal{G}_I = \lim_{\Delta c \to 0} \frac{1}{2\Delta c} \int_0^{\Delta c} \sigma_{22}(\Delta c - r, 0) v(r, \pi) dr, \tag{39}$$

where σ_{22} is the normal component of the Cauchy stress ahead of the crack tip, v is the opening displacement between points on the crack faces behind the crack tip and Δc is the crack extension. The physical interpretation of the integral in equation (39) is the amount of work required to close the crack by Δc [22].

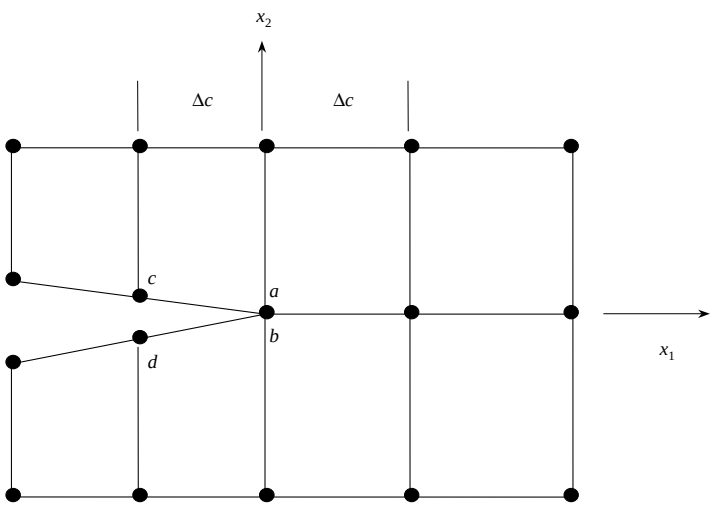

Fig. 11. Finite element mesh near the crack tip.

The schematic of the finite element mesh near the crack tip is shown in Fig.11. It corresponds to the boxed region in Fig.9. In terms of the finite element representation, $\mathcal{G}_I$ is one-half of the product of the forces at nodes c and d (F_c) required to close these nodes, multiplied by the opening displacement, i.e.

$$\mathcal{G}_I = \lim_{\Delta c \to 0} \frac{1}{2\Delta c} F_c (v_c - v_d). \tag{40}$$

Following [22], the lengths of the elements ahead and behind the crack tip are selected to be equal and a very stiff spring element is placed between nodes a and b, which enables us to make the approximation that the force F_c required for crack closure is equal to the nodal force F_a (spring force).

The following material parameters are used for the numerical calculations (subscripts 1 and 2 correspond to TiO_2 and Ti-15-3, respectively) :

(1) For the oxidation problem (700°C) [23]:
- Diffusivity coefficients: $D_1 = 3.02 \cdot 10^{-3} \mu m^2/s$, $D_2 = 1.431 \cdot 10^{-3} \mu m^2/s$;
- Critical value of the oxygen concentration: $c_{cr} = 0.65 c_0$;
- Concentration jump across the interface: $[c] = 0.5 c_0$.

(2) For the mechanical problem (room temperature) [31]:
- Young's modulus: $E_1 = 18.2 GPa$, $E_2 = 11.4 GPa$;
- Poisson's ratio: $\nu_1 = \nu_2 = 0.3$.

Four different values of volumetric expansion of the oxide scale are used in this section. The volumetric expansion is modeled by an eigenstrain, i.e., $\varepsilon_{ij} = \varepsilon^e_{ij} + \varepsilon^v \delta_{ij}$, where ε_{ij} is the total strain in the oxide, ε^e_{ij} is the elastic strain and ε^v is the volumetric eigenstrain. The finite element mesh used for numerical computations is shown in Fig.8b (the mesh consists of 1689 elements). Results, obtained with the crack closure method for an applied force of $1.0 \cdot 10^6 N$, are plotted in Fig.12. The numerical results presented here for the mechanical problem are derived using the commercial finite element software ABAQUS while the calculations for the moving oxidation front have been performed by an in-house developed finite element code, based on the formulation described in section 3.2.

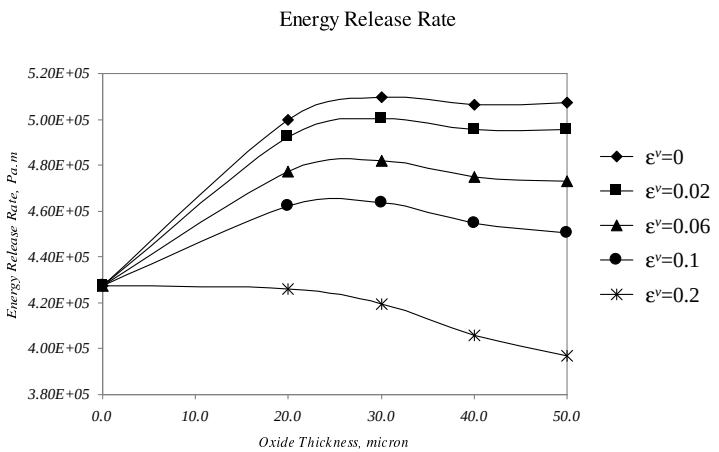

Fig. 12. Energy release rate for different values of volumetric expansion.

As it can be seen in Fig.12, the change in the stiffness due to oxide scale formation increases the energy release rate as the oxide grows. The volumetric expansion in the oxide scale, which causes an initial compressive stress field near the crack tip (see Fig.13), decreases the energy release rate.

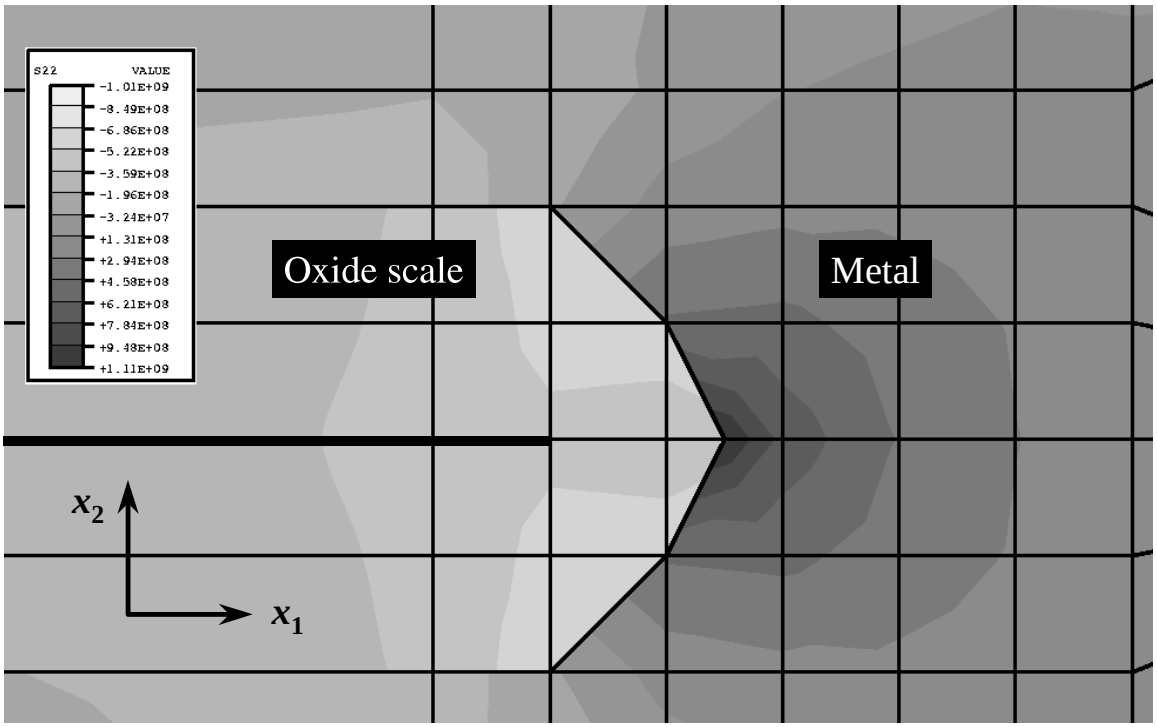

Fig. 13. Contour plot of σ_{22} near the crack tip for oxide thickness of $20\mu m$ with volumetric expansion of 10% ($\varepsilon^v = 0.1$) and no externally applied load.

5 Conclusions

An effort to investigate the effect of oxidation on the crack growth resistance of titanium alloys has been done by modeling the oxidation and energy release rate of compact tension specimens.

Two variants of fixed grid finite element method for simulation of the oxidation in titanium alloys have been derived from two different concepts (i.e., the discrete interface method and the smearing front method). Both approaches have been tested on problems that have analytical solution (i.e., 1-D oxidation and 2-D ordinary diffusion) and have shown very good accuracy. Validated numerical models have been used to simulate the oxide growth from the crack surface in Ti-15-3 alloy. The crack closure method has been implemented and has been used to calculate the energy release rate of Ti-15-3 compact tension specimen. In the finite element formulation of the mechanical problem, the influence of oxidation has been introduced by the change of the elastic constants and the oxidation-induced eigenstrain. The oxidation and mechanical models have been applied to simulate oxidation of a pre-cracked Ti-15-3 compact tension specimen which is then subjected to monotonic loading.

Exact knowledge of the eigenstrain, developed during the oxidation, prevented us from a

direct comparison of modeling results with experimental observations. In the case that accurate measurement of the eigenstrain can be established, the developed procedure could be used to estimate the critical energy release rate for given oxide thickness by comparing with experimental results (critical load for crack growth). Future work will focus on measuring the volumetric expansion during oxidation and introducing it into the oxidation modeling. The ultimate goal is to fully couple the oxidation with the mechanical problem, so that oxide growth under applied loading at an elevated temperature can be modeled.

Acknowledgments — The authors wish to express appreciation for the support provided by AFOSR grants No.F49620-94-1-0341 and No.F49620-97-1-0338. The authors also acknowledge P.K.Imbrie and David Miller for the SEM photographs of the oxidized specimens.

References

[1] D.H. Allen, M.R. Eggleston, and L.D. Hurtardo. Recent research on damage development in SiC/Ti continuous fiber metal matrix composites. In E.A. Armanios, editor, *Fracture of Composites*, Key Engineering Material. Trans Tech Publications. To appear.

[2] L.A. Wittig and D.H. Allen. Modeling the effect of oxidation on damage on SiC/Ti-15-3 metal matrix composites. *J. of Engr. Matls. and Tech.*, 116:421–427, 1994.

[3] B.A. Lerch, T.P. Gabb, and R.A. Mackay. Heat treatment study of the SiC/Ti-15-3 composite system. Technical Report TP-2970, NASA, 1990.

[4] P. Bartolotta and M.J. Verrilli. Thermomechanical fatigue behaviour of SiC/Ti-24Al-11Nb in air and argon environments. Technical Report TM-105723, NASA, 1992.

[5] W.C. Revelos, J.W. Jones, and E.J. Dolley. Thermal fatigue of SiC/Ti-15Mo-2.7Nb-3Al-0.2Si composite. *Metallurgical and Materials Transaction*, 26A:1167–1181, 1995.

[6] J.M. Foulk. A model for predicting the damage and oxidation dependent life of SCS-6/TI-β21S[0] metal matrix composite. Master's thesis, Texas A&M University, College Station, TX., 1997.

[7] D.C. Lagoudas, S. Xu, D. Miller, and D.H. Allen. Damage in oxidized titanium metal matrix composites. In *Proceeding of the ASME Aerospace and Material Divisions, 1996 ASME International Mechanical Engineering Congress and Exposition*, volume 73, pages 225–237, 1996.

[8] Michael G. Castelli. Isothermal damage and fatigue behavior of SCS-6/TIMETAL 21S$[0/90]_s$ composite at 650°C. *Composites*. In review.

[9] J. Gayda and T. P. Gabb. Isothermal fatigue behavior of a $[90]_8$ SiC/Ti-15-3 composite at 426°C. *International J. of Fatigue*, pages 14–20, January 1992.

[10] Andrew H. Rosenberger and Theodore Nicholas. Environmental effects on the isothermal and thermomechanical fatigue of SCS-6/TIMETAL 21S unidirectional composite. In E. A. Armanios, editor, *Composite Materials: Fatigue and Fracture (Sixth Volume)*, volume ASTM STP 1285, pages 394–408. American Society for Testing and Materials, 1997.

[11] Michael G. Castelli and J. Gayda. An overview of elevated temperature damage mechanisms and fatigue behavior of a unidirectional SCS-6/Ti-15-3 composite. *Reliability, Stress Analysis, and Fatigue Prevention*, DE-55 ASME:213–221, September 1993.

[12] A. H. Rosenberger. Effect of vacuum level on the embrittlement of TIMETAL 21S. *Scripta Materialia*, 34(12):1877–1882, 1996.

[13] Andrew H. Rosenberger, B. D. Worth, and J. M. Larsen. Effects of microstructure, temperature and environmental on fatigue crack growth in Ti-46.5Al-3NB-2Cr-0.2W γ titanium aluminide. In M.V. Nathal, R. Darolia, C.T. Liu, P.L. Martin, D.B. Miracle, R. Wagner, and M Yamaguchi, editors, *Structural Intermetallics 1997*, pages 555–561. The Minerals, Metals & Materials Society, 1997.

[14] Stephan M. Russ, Andrew H. Rosenberger, and David A. Stubbs. Isothermal fatigue of SCS-6/Ti-22Al-23NB composite in air and vacuum. In S.R. White, H.T. Hahn, and W.F. Jones, editors, *Recent Advances in Composite Materials*, pages 13–22. ASME, New York, 1995.

[15] J. Ferreira, E. Aghion, and N. Comins. High temperature fatigue crack growth behavior of Timetal-21S in an oxidizing environment, 1997. Mechanical Engineering Department, University of Natal, Durban, 4001, South Africa.

[16] J. Douglas and G.M. Gallie. On numerical integration of a parabolic differential equations subject to a moving boundary. *Duke Math. J.*, 22(4):557–572, 1995.

[17] F.P. Vasil'ev and A.B. Uspenskii. Finite-difference solution of the two–phase Stefan problem. *USSR Comput. Math. & Math. Phys.*, 3(5), 1963.

[18] J.C. Chen and Y.C. Huang. Thermocapillary flows of surface melting due to a moving heat flux. *Int. J. Heat Mass Transfer*, 33:1165–1175, 1990.

[19] M.G. Worster. Solidification of an alloy from a cooled boundary. *J. Fluid Mech.*, 167:481–501, 1986.

[20] V.K. Manolov, O.P. Iliev, and I.V. Bizhev. Numerical simulation of nitrogen diffusion in a solid chromium particle. *Journal of Theoretical and Applied Mechanics*, 24, 1993.

[21] A.A. Samarskii and B.D. Moiseenko. An economic continuous calculation scheme for the Stefan multidimensional problem. *USSR Comput. Math. & Math. Phys.*, 5(5):43–58, 1965.

[22] E.F. Rybicki ans M.F. Kanninen. A finite element calculation of stress intensity factors by a modified closure integral. *Engineering Fracture Mechanics*, 9:931–938, 1977.

[23] D.C. Lagoudas, X. Ma, D.A. Miller, and D.H. Allen. Modeling of oxidation in metal matrix composites. *Int. J. Engng Sci.*, 33(15):2327–2343, 1995.

[24] J.N. Reddy. *An Introduction to the Finite Element Method.* McGraw-Hill Inc., 1993.

[25] P.B. Entchev. Algorithms for solving phase change free boundary problems : a review. Technical report, Bulgarian Academy of Sciences, 1995. Unpublished.

[26] D. C. Lagoudas, P. B. Entchev, and R. H. Triharjanto. Modeling of oxidation and its effect on the crack growth resistance of titanium alloys. In G.Z. Voyiadjis, editor, *Studies in Applied Mathematics: Volume on Damage Mechanics in Engineering Materials.* Elsevier Science, 1998. To appear.

[27] R.S. Barsoum. On the use of isoparametric finite element in linear fracture mechanics. *Int. J. for Numerical Methods in Engng.*, 10:25–37, 1976.

[28] K. Hellan. *Introduction to Fracture Mechanics*. McGraw-Hill Inc., 1984.

[29] J. R. Rice. Mathematical analysis in the mechanics of fracture. In H. Liebowitz, editor, *Fracture, an Advanced Treatise*, chapter 3, pages 192–311. Academic Press, 1968.

[30] P.S. Steif. A semi-infinite crack problem partially penetrating a circular inclusion. *Journal of Applied Mechanics*, 54:87–92, 1987.

[31] J.C. Fanning. Ti-15-3 property data. In *Beta Titanium Alloys in the 1990's, Proceeding of Harold Margolin Symposium on Microstructure/Property Relationship of Titanium Alloys*, pages 411–438, Denver, Colorado, 1993. The Minerals, Metals and Matertials Society.

Appendix

A On the Applicability of the Isoparametric Method for Oxidation Problems

In many oxidation problems, the oxide scale covers the whole surface area of the crack, as schematically shown in Fig.10. For such cases the isoparametric method for the evaluation of the energy release rate is not applicable, as discussed in Section 4. Indeed, there is an infinite number of values for the J-integral, depending on the selection of the integration path (Fig.10). However, if the oxide scale partially covers the crack surfaces, as schematically shown in Fig.A.1, there are two distinct values of the J-integral, one for paths inside the oxide scale (Γ_2) and the other for paths outside the oxide scale (Γ_1). For the case of

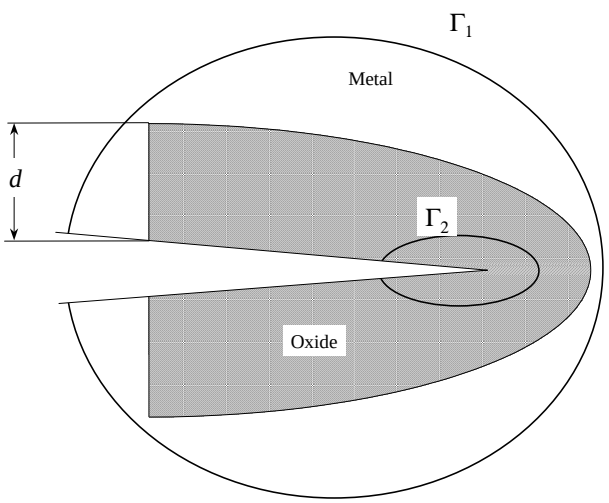

Fig. A.1. Schematic representation of an oxidated cracked specimen with oxide layer partially covering crack surfaces.

the inhomogeneity being of circular shape, analytical results have been reported in [30]. We have used the results reported in [30] to validate our numerical implementation of the isoparametric method.

An example of the implementation of the isoparametric method for confined oxidation around a crack tip is given in Fig.A.2. The normalized value of the J-integral for paths inside and outside of the oxide scale for the above problem and for volumetric expansion corresponding to 0.05% as a function of the thickness d of oxide scale is shown in Fig.A.3. In the same figure the results of the crack closure method have also been reported and they coincide with the values of the J-integral inside the oxide scale.

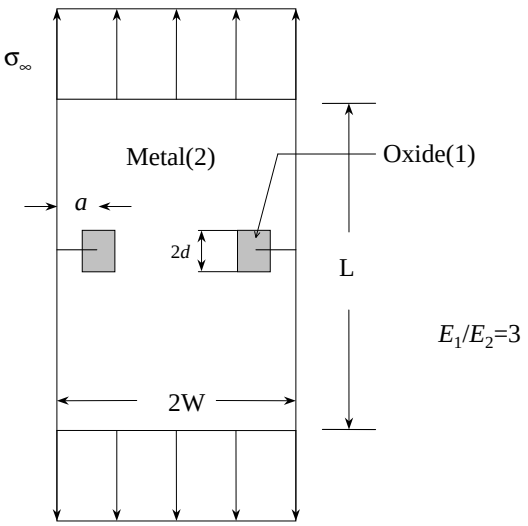

Fig. A.2. Schematic of the problem involving square oxide inclusion.

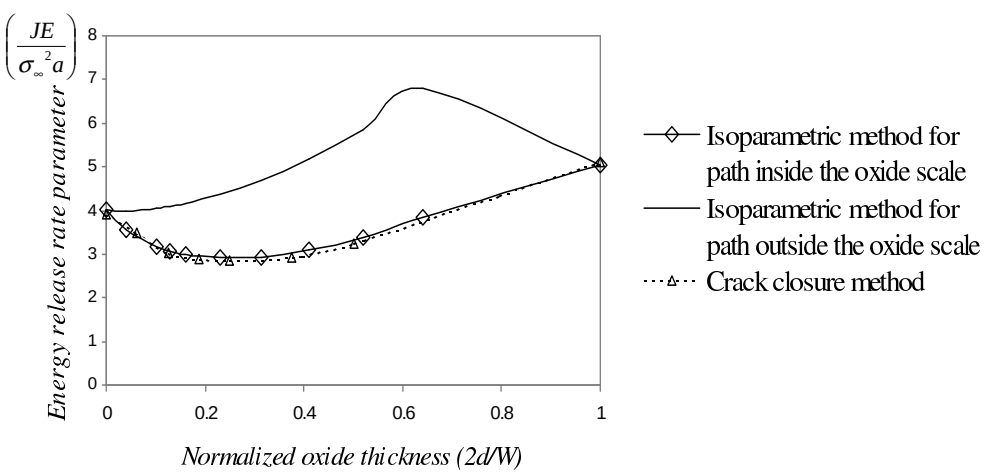

Fig. A.3. Energy release rate vs. oxide thickness.